J. Micromech. Microeng. **17** (2007) 1034–1041 doi:10.1088/0960-1317/17/5/025

A 1 × 2 optical fiber switch using a dual-thickness SOI process

Yao-Joe Yang, Wen-Cheng Kuo, Kuang-Chao Fan and Wu-Lang Lin

Department of Mechanical Engineering, National Taiwan University, No 1 Roosevelt Rd, Sec. 4, Taipei, Taiwan, Republic of China

E-mail: yjy@ntu.edu.tw

Received 28 December 2006, in final form 19 March 2007
Published 17 April 2007
Online at stacks.iop.org/JMM/17/1034

Abstract

This work presents a micro-electro-mechanical system 1 × 2 optical fiber switch fabricated by a dual-thickness SOI process. The switch employs a fiber-switching mechanism which consists of comb-drive actuators and folded-beam suspensions. The design and modeling of the fiber-switching mechanism, which can effectively avoid electrostatic pull-in, is also presented. The device is realized by using a dual-thickness SOI process which can be used to create suspended microstructures with two different structure thicknesses. The measured average insertion losses for the two output channels are 0.92 dB and 0.89 dB, which satisfy the BELLCORE requirements. Also, the transient behaviors are measured. The typical switching time is about 3.5 ms.

(Some figures in this article are in colour only in the electronic version)

1. Introduction

Optical fiber switches play an important role in optical fiber communication for mapping wavelengths from input ports to appropriate output ports based on the destinations. Conventional optical switches are of the optic-electro-optic (O-E-O) type, and have many drawbacks. For example, they require expensive optic-electro conversion devices. The signal loss and crosstalk between each channel are usually noticeable. Also, the electronics bottleneck constrains the growth in the capacity of the optics as the required bandwidth is increased. The all-optic switching (O-O-O) design can potentially eliminate these disadvantages, and is compatible with dense wavelength division multiplexing (DWDM) technology, such that it is suitable for use in the next generation of optical switching technology [1].

Many all-optical switching designs for micro-electro-mechanical system (MEMS) optical switching mechanisms have been developed. There are two major types of switching designs: the light-beam-switching design [2] and the fiber-switching design [3], as illustrated in figure 1. The light-beam-switching design needs to use light-beam-focusing components, such as collimators, lensed fibers and microlens, to shape the beam of radiation emerging from the light source and to limit the maximum field size of light beams. Then light beams are reflected by micromirrors from the input channels to the output channels to achieve switching. The fiber-switching design, on the other hand, uses actuators to move fibers directly to switch light from one channel to the other. Table 1 illustrates the comparison between the light-beam-switching design and the fiber-switching design. When compared with the light-beam-switching design, the fiber-switching design is restricted to the devices with a small array size (1 × 2 and 1 × 4 [8]). However, as indicated in table 1, the fiber-switching design gives very low insertion loss. Also, it does not require light-beam-focusing components, which in turn makes the system relatively of low cost and easy to assemble. Therefore, the fiber-switching design is indeed a very competitive approach for optical fiber switches of small array sizes (1 × 2 or 1 × 4 systems).

Various MEMS fiber-switching designs for 1 × 2 optical switches have been proposed, such as the SDA cam-micromotor type [9], shape-memory-alloy (SMA) type [10], micro-magnetic-alloy-pipe type [11], electrostatic-parallel-plate type [12], bistable-thermal-actuation type [13] and magnetic-actuation type [14, 15]. There are some issues among these types of designs. For example, the SDA actuator [9] has the well-known undesirable wear problem which

Table 1. A comparison of MEMS optical switches using the light-beam-switching design and the fiber-switching design.

	Switching designs		
	Light beam-switching		Fiber-switching
Requirement of mirrors	Yes		No
Requirement of light beam focusing	Yes		No
Light beam focusing component	Collimator (Koncent Inc. [4])	Lensed fiber/microlens (Corning Inc. [5])	None
Distance of motion for actuators	$\geqslant$500 μm [4] (typical) (Minimum light-beam width in free space)	$\geqslant$18 μm [5] (typical) (Minimum light-beam width in free space)	125 μm (Fiber outer diameter without cladding)
Working distance[a]	>5000 μm [4] (typical)	<300 μm [5] (typical)	<10 μm (typical)
(a) Mirror loss[b]	$\geqslant$0.2 dB [6]	$\geqslant$0.2 dB [6]	None
(b) Coupling loss[b]	$\geqslant$0.15 dB [4]	$\geqslant$0.3 dB [5]	$\geqslant$0.1 dB [7] (10 μm working distance)
(a) + (b) = insertion loss[b]	$\geqslant$0.35 dB	$\geqslant$0.5 dB	$\geqslant$0.1 dB

[a] Working distance is the free-space distance of the light beam between input and output ports.
[b] The values of losses in the table are obtained under the condition of perfect alignment of fibers.

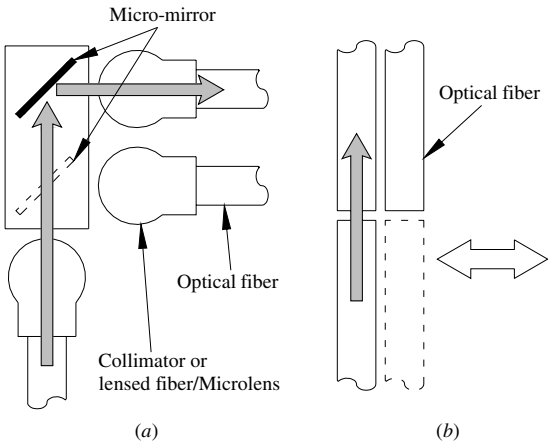

Figure 1. (*a*) A schematic view of the light-beam-switching design and (*b*) the fiber-switching design.

prohibits long-term applications [16]. The switching time of the SMA actuator [10] and the thermal actuator [13] is relatively slow (>100 ms). Also, although the parallel plate actuator [12] can generate a large lateral displacement for fiber switching, it requires a larger structure length (die size is about 35 mm × 1.5 mm) and structure thickness (~500 μm) in order to generate adequate force and to reduce the axial and angular misalignment for butt coupling. Furthermore, in [10, 11, 14, 15], since the devices require magnetic coils or magnets for actuation, the fabrication and assembly processes are relatively complicated. In this work, we also employ the fiber-switching design as the switching mechanism of our optical fiber switch. Our proposed device is the first one to successfully integrate comb-drive actuators and folded-beam flexures [17] as a fiber-switching mechanism. The design can achieve the requirement of a large displacement with a small switching time. Also, the proposed design gives a small sideward displacement which is essential for fiber alignment. Also, this design has relatively smaller footprint (die size is about 15 mm × 13 mm). Finally, a novel dual-thickness SOI micromachining technique, which is quite simple and inexpensive, is also proposed for fabrication of the device.

This paper is organized as follows: the micromechanism design for the proposed device is described in section 2. Section 3 presents the fabrication process. Measured results are presented in section 4. Finally, section 5 draws conclusions.

2. Design of the fiber-switching mechanism

Figure 2 schematically depicts the proposed 1 × 2 optical fiber switch which employs the fiber-switching design. The device consists of a suspended fiber-holding table, folded-flexures and two comb-drives. All of the components can be monolithically fabricated using the dual-thickness SOI process which will be described in the next section. In order to achieve a displacement of about 125 μm, which is required for the fiber-switching design, the suspension beams must be very flexible to produce a relatively large displacement under a reasonable driving voltage. Also, the inter-digital comb fingers should move only in the desired lateral direction with a minimal sideward movement. Doing so requires a large stiffness ratio between the sideward spring constant and the lateral spring constant. Various suspension designs, including clamped–clamped beam design, crab-leg flexure design and folded-flexure design, displayed in figure 3, have large stiffness ratios. Among these designs, folded-flexure design is the best because of the following reasons: (1) it offers a large linear deflection range as well as a high stiffness ratio between sideward and lateral spring constants [18], which effectively prevents electrostatic pull-in; (2) it gives relatively smaller axial and angular misalignment associated with butt coupling. Also, stoppers are used for precise radial alignment to ensure a low butt-coupling loss between the input fiber and the output fiber.

As shown in figure 4(*a*), when the left comb-drive is actuated, the holding table is driven to come into contact with the left stopper with a stroke of 62.5 μm (fiber radius). The stopper is used to align the input fiber and the output fiber for channel 1. Similarly, figure 4(*b*) schematically depicts the actuation of the right comb-drive. Accordingly, 1 × 2 optical switching can be achieved by alternating the actuation of the comb-drive actuators.

The actuation force generated by the comb-drive actuator is given by

$$F = 2N\left(\frac{1}{2}\varepsilon_0 V^2\right)\left(\frac{H_{\text{beam}}}{z_{\text{gap}}}\right), \tag{1}$$

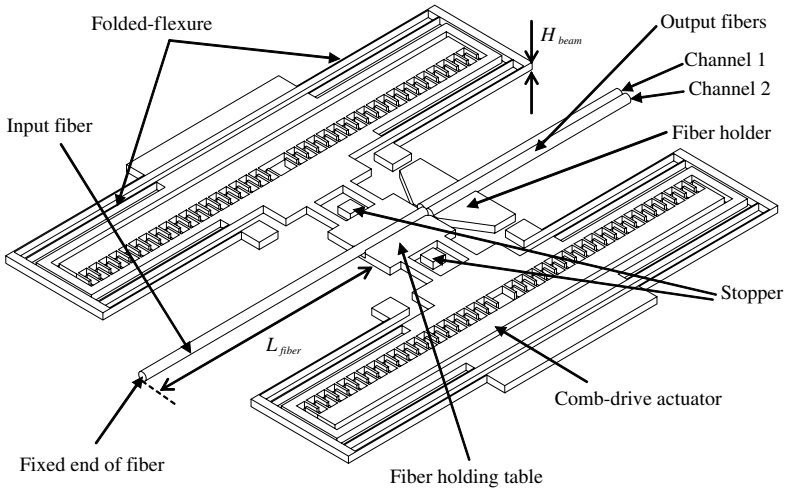

Figure 2. A schematic of the proposed 1 × 2 optical fiber switch at a neutral position.

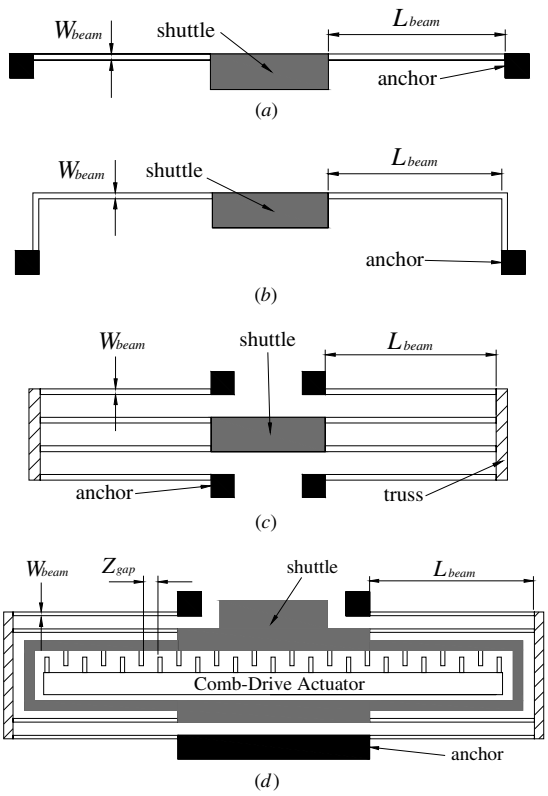

Figure 3. (*a*) A schematic view of the clamped–clamped beam design, (*b*) the crab-leg flexure design, (*c*) the folded-flexure design and (*d*) the folded-flexure integrated with comb-drive actuator design.

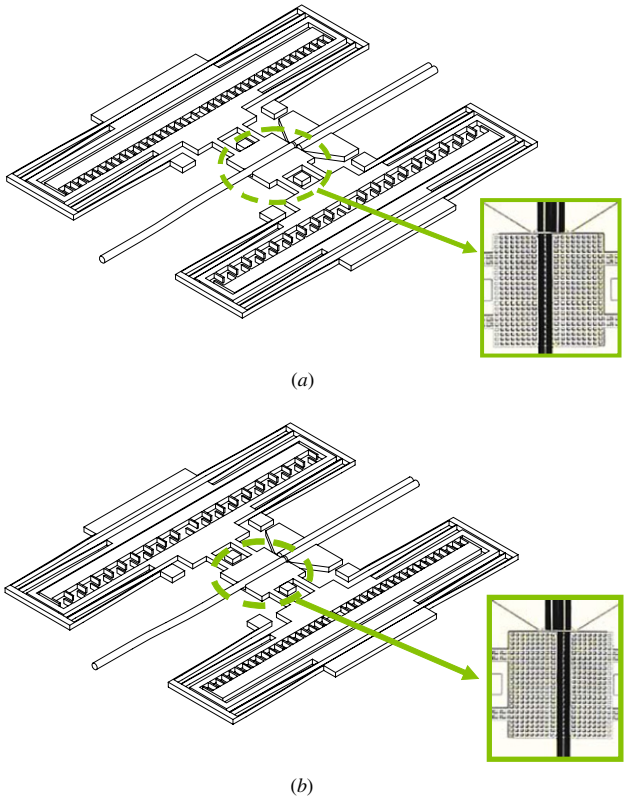

Figure 4. Schematic views and CCD pictures of the switch at different switching positions: (*a*) the left comb-drive is actuated and (*b*) the right comb-drive is actuated.

where N denotes the number of comb finger pairs, ε_0 is the permeability of free space (8.85×10^{-12} F m^{-1}), V is the applied voltage, H_{beam} is the thickness of comb fingers and folded beams, and z_{gap} is the gap between the comb fingers.

Simple beam theories can be used to estimate the mechanical characteristics of the folded beams [19, 20]. The lateral stiffness of folded beams is

$$k_{\text{folded}} = \frac{48E_{\text{Si}}\left[H_{\text{beam}} \cdot W_{\text{beam}}^3/12\right]}{L_{\text{beam}}^3}, \tag{2}$$

where E_{Si} is Young's modulus of silicon (175 GPa), W_{beam} is the width of the folded beam and L_{beam} is the length of the beam.

Since the optical fiber switch must drive the switching of the input fiber, the stiffness of the input fiber must be considered. The lateral stiffness of the input fiber k_{fiber} is given by

$$k_{\text{fiber}} = \frac{12E_{\text{fiber}}\pi r^4}{L_{\text{fiber}}^3}, \tag{3}$$

where E_{fiber} is Young's modulus of the optical fibers (70 GPa),

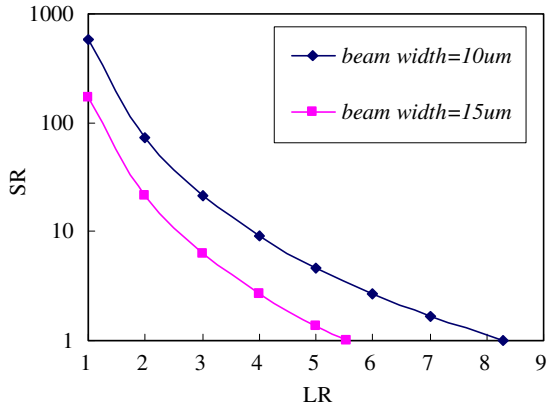

Figure 5. Relationships between the stiffness ratio (SR) of fiber/folded beams and the length ratio (LR) of fiber/ folded beams. The beam thickness is 100 μm.

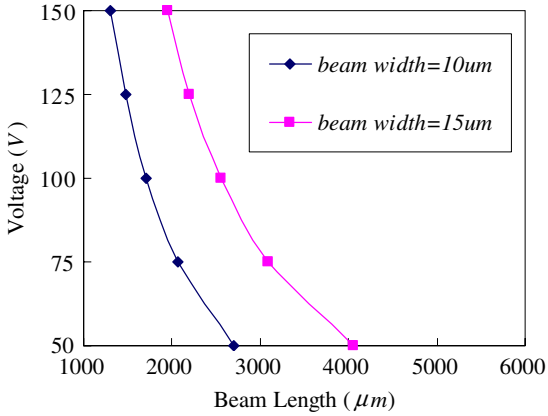

Figure 6. Relationships between the required applied beam length versus voltage for various beam widths, for achieving a displacement of 62.5 μm. Note that the gap is 5 μm, the beam thickness is 100 μm and the number of finger pairs is 1000. Also, the length ratios (fiber/folded beams) are 5.5 and 8.3 for the beam widths of 15 μm and 10 μm, respectively.

r is the radius of the input fiber and L_{fiber} is the suspended length of the input fiber.

The total stiffness (k_{total}) for lateral motion is

$$k_{\text{total}} = k_{\text{folded}} + k_{\text{fiber}} = \frac{48E_{\text{Si}}\left[H_{\text{beam}} \cdot W_{\text{beam}}^3/12\right]}{L_{\text{beam}}^3} + \frac{12E_{\text{fiber}}\pi r^4}{L_{\text{fiber}}^3}. \quad (4)$$

The force required for a fiber-switching distance up to 62.5 μm (D) is

$$F = k_{\text{total}} \cdot D. \quad (5)$$

Equations (1) and (4) can be used to rewrite equation (5) as

$$V = \sqrt{\frac{4z_{\text{gap}}D}{\varepsilon_0 N H_{\text{beam}}}\left(\frac{E_{\text{Si}}H_{\text{beam}}W_{\text{beam}}^3}{L_{\text{beam}}^3} + \frac{3E_{\text{fiber}}\pi r^4}{L_{\text{fiber}}^3}\right)}. \quad (6)$$

The height of the device (H_{beam}) is 100 μm to ensure that the fiber-holding table is sufficiently stiff. Figure 5 shows the relationship between the length ratio (LR) and the stiffness ratio (SR) for the fiber and the folded beams. When the lengths of the fiber and the beam are the same (length ratio is equal to 1), the stiffness of the fiber will be at least two orders larger than that of the folded beams. For the beam with a width of 10 μm, the stiffness ratio reaches 1 when the length of fiber is 8.3 times as that of the beam. Similarly, for the beam with a width of 15 μm, the stiffness ratio reaches 1 when the length ratio is 5.5. The length ratios of 5.5 and 8.3 are chosen for the beam widths of 15 μm and 10 μm, respectively, so that the stiffness of the folded beams and the stiffness of the fiber will be the same. Note that since the radius of the fiber is 62.5 μm, the fiber mounting grooves of the fiber holder and fiber-holding table are designed to be 65 μm deep.

Figure 6 plots the relationships between the folded-beam length (L_{beam}) and the applied voltage (V) at various beam widths (W_{beam}) for a generated displacement of 62.5 μm. The required applied voltage decreases as the beam length increases. Besides, a wider beam must also be longer to maintain the same applied voltage. Based on the constraint of fabrication capacity for the large device thickness (~100 μm) of suspended structures with a driving voltage of 100 V, the designed device dimensions are listed in table 2. Note that the length ratios (fiber/folded beams) are 5.5 and 8.3 for the beam widths of 15 μm and 10 μm, respectively. With these length ratios, the folded-beam stiffness will be the same as the effective stiffness of the input fiber (i.e. SR ratio is equal to 1). In fact, the SR ratio can be other value rather than 1. However, if the SR ratio is much greater than 1, we might need much higher applied voltage than the typical devices with similar sizes. On the other hand, if the SR ratio is much less than 1, the total device length has to be increased significantly in order to accommodate the fixed end of the input fiber (the movable fiber). We set the SR ratio as 1 to easily estimate the applied voltages for a device with a reasonable size (about 15 mm × 13 mm).

Table 2. The designed device dimensions of the 1 × 2 optical switch.

Parameters	Values
Device thickness	100 μm
Gap between comb fingers	5 μm
No of pairs of comb fingers	1000
Folded-beam length	2557 μm
Folded-beam width	15 μm
Input fiber length	14.2 mm

The switching time of the device can be approximately estimated using the following formula [7]:

$$T = \frac{\pi}{2}\sqrt{\frac{M_{\text{shuttle}} + \frac{1}{2}M_{\text{truss}} + \frac{96}{35}(M_{\text{beam}} + M_{\text{input fiber}})}{k_{\text{Total}}}}, \quad (7)$$

where M_{shuttle} is the mass of the shuttle which includes the fiber moving table, M_{truss} is the mass of the truss, M_{beam} is the mess of beam and $M_{\text{input fiber}}$ is the mass of suspended input fiber, as displayed in figures 2 and 3.

The estimated switching time is approximately 4.2 ms and satisfies the requirement of the BELLCORE standard [21] (<20 ms).

3. Fabrication

Since the thickness of the device is designed to be 100 μm and the depth of the fiber mounting groove is 65 μm, bulk

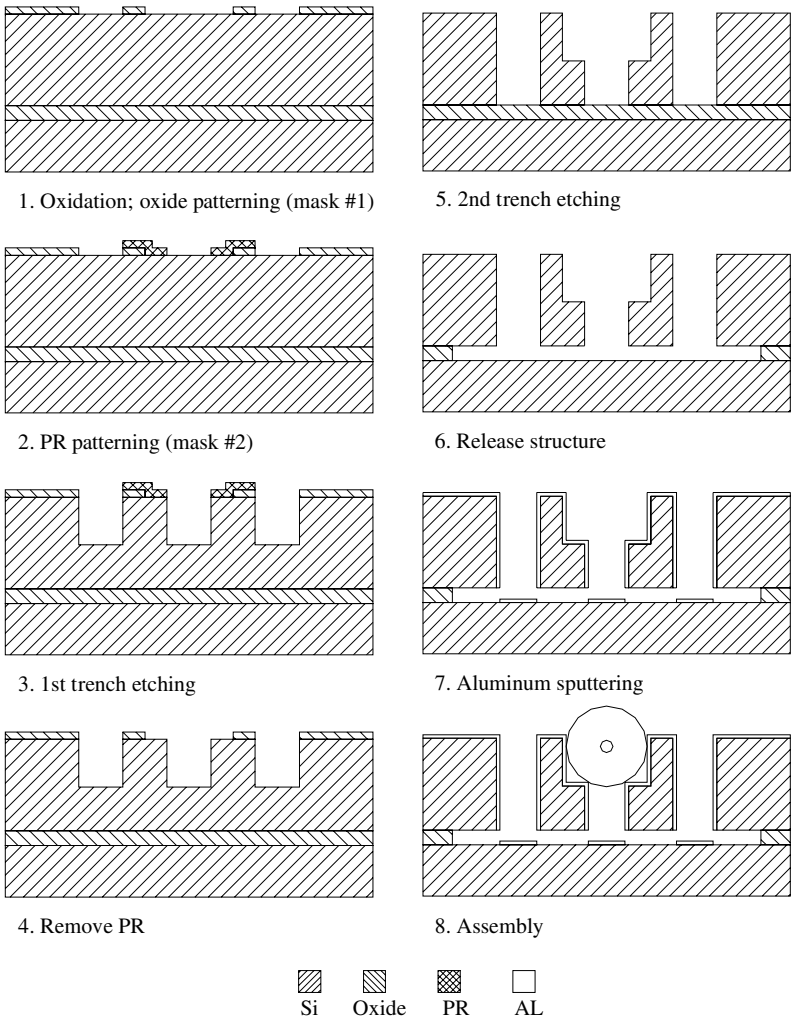

Figure 7. The dual-thickness SOI fabrication process for the 1 × 2 optical fiber switch. Note that the process employs ICP etching on a SOI wafer patterned with two layers of etching masks for fabricating a dual-thickness structure.

micromachining technology must be utilized to fabricate the device. The gap between comb fingers is 5 μm and the maximum trench aspect ratio is 20. For fabricating suspended microstructures with high aspect ratios, the SOI process is one of the most popular approaches because of its simplicity. The former designs [10, 11, 14, 15] need additional steps for part assembly. In order to reduce the complexity of fabrication and assembly, a novel dual-thickness SOI process is proposed to fabricate the suspended structure with layers of two different thicknesses. This process can monolithically create most of the parts of the device (folded-flexures, comb-drive actuators, stoppers, fiber holder and fiber-holding table) without the assembly process. The thicker layer serves as the structure layer, and thinner layer serves as the fiber mounting grooves.

Figure 7 shows the manufacturing process. In the first step, 1 μm silicon oxide is grown on an SOI wafer, and is then patterned using the first mask. The second mask is then used to pattern the photoresist AZ4620 to define the fiber-holding grooves (the second step). The third step is the first trench etching (the Bosch process [22]). The STS ICP–RIE system is used to etch the substrate to a depth of 35 μm. In the fourth step, the photoresist AZ4620 is removed by oxygen plasma and the silicon surface is exposed for the following fiber mounting grooves etching. The fifth step is the second trench etching, in which the fiber mounting grooves are etched to a trench depth of 65 μm, and other trenches are etched to 100 μm. Note that the third, the fourth and the fifth steps can be integrated into a single ICP–RIE run. In the sixth step, HF solution is used to release the structure. In the seventh step, a conductive layer is sputtered for further electrostatic actuation. Finally, by using precision holders, the optical fibers are put into the fiber mounting grooves on the fiber holder and on the fiber moving table. This step is assisted by using a charge-coupled device (CCD) camera to check the locations of the fibers. The alignment of the fibers is performed until the insertion losses of both channels meet the BELLCORE requirement. Then the fibers are fixed by UV glue. Note that the distance between the input fiber and the output fiber is less than 10 μm in the axial direction to reduce the coupling loss [7].

4. Measurements and results

The outer diameter and the core diameter of the multimode optical fibers used in this work are 125 μm and 62.5 μm,

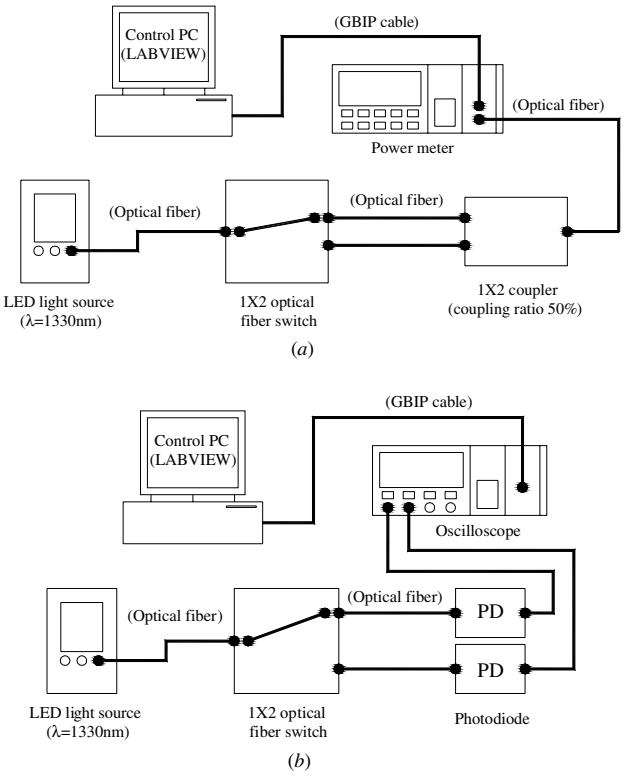

Figure 8. A schematic of the optical measurement setup (*a*) for measuring insertion losses and (*b*) for measuring transient switching behaviors.

respectively. Also, there is no antireflective coating, and zero cut-angle on the fiber tip. In this work, an optical power meter is used to measure the insertion loss, and photodiodes are used to measure the transient switching behaviors. The schematics of the measurement setup are presented in figures 8(*a*) and (*b*).

In figure 8(*a*), a 1310 nm LED (EXFO-FLS-300) serves as the light source. A coupler (FOCI-Multimode, coupling ratio = 50%) is connected on the two output channels of the switch so that the switching optical signals from the two channels can be measured by the power meter (Anritsu-Mu931421A). In figure 8(*b*), the signals of the two output channels are measured by two photodiodes (EZconn-ESR709). Note that the output currents of the photodiodes are converted into voltages by simple amplification circuits.

The trench aspect ratio of fabricated optical fiber switches is as high as 20. Figures 9 and 10 show the scanning electron micrograph (SEM) and the optical photograph of the device structures. Figure 11(*a*) shows the packaged 1 × 2 optical switch, and figure 11(*b*) is the close-up view of the packaged optical switch (no cap).

Without the application of electrostatic voltage, the holding table and the input fiber are in the middle position (neutral position). When the left comb-drive actuator is actuated (100 V), the holding table is driven to the left and touches the left stopper; then the input fiber aligns with the output fiber (channel 1), as shown figure 4(*a*). When the right comb-drive actuator is actuated with 100 V (and the left comb-drive is not actuated), the holding table is driven to the right and touches the right stopper; then the input fiber aligns with the output fiber (channel 2), as shown in figure 4(*b*). Note that

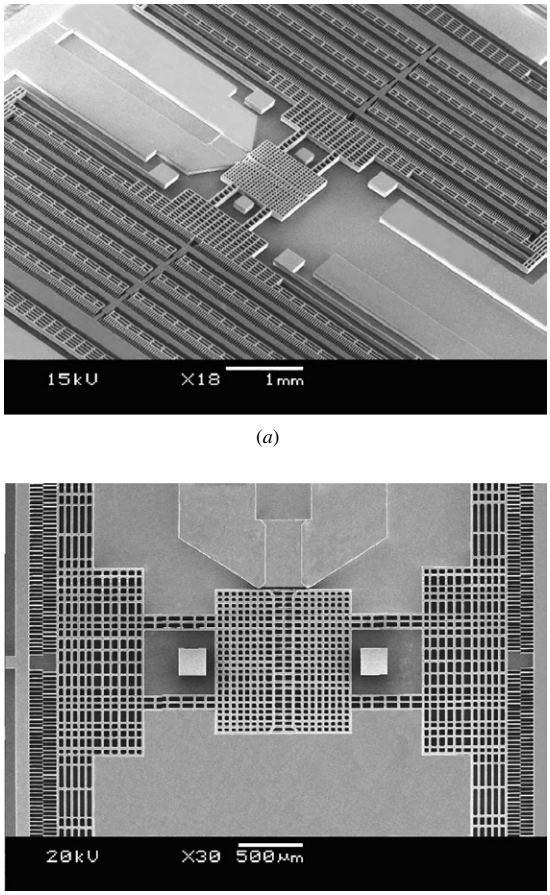

Figure 9. A SEM micrograph of a 1 × 2 optical fiber switch.

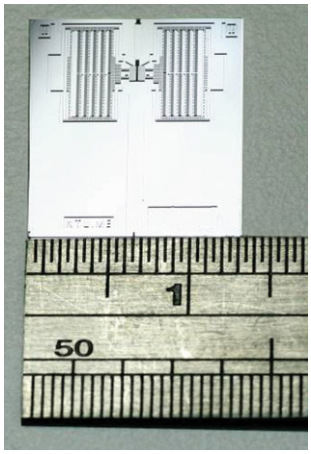

Figure 10. A picture of a 1 × 2 optical fiber switch without fiber assembly.

the pictures in the right-bottom corner of figures 4(*a*) and (*b*) are the CCD photographs of the device in the corresponding status. The measured average insertion losses for channels 1 and 2 are about 0.92 dB and 0.89 dB, respectively. The corresponding deviations for the two channels are 0.06 dB and 0.06 dB.

Figure 12 shows the measured switching behaviors of the voltage output signals of channels 1 and 2 obtained using the

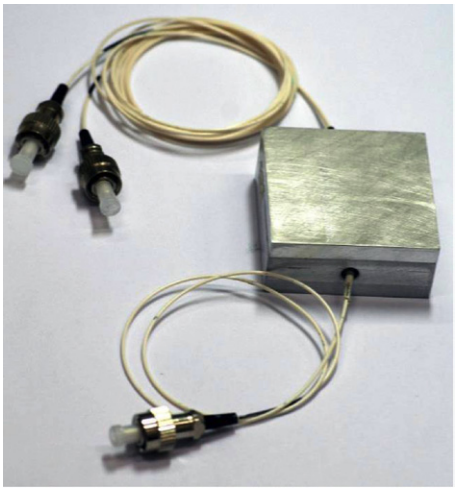

(*a*)

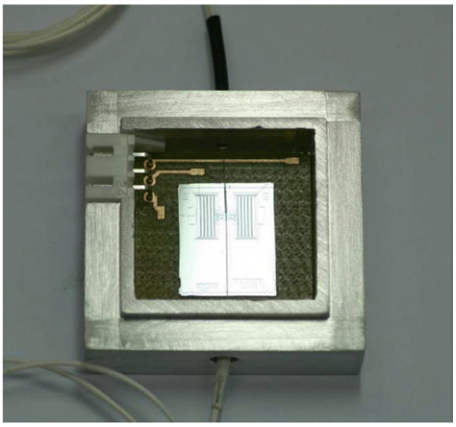

(*b*)

Figure 11. (*a*) A packaged 1 × 2 optical switch and (*b*) a close-up view of the packaged optical switch (no cap).

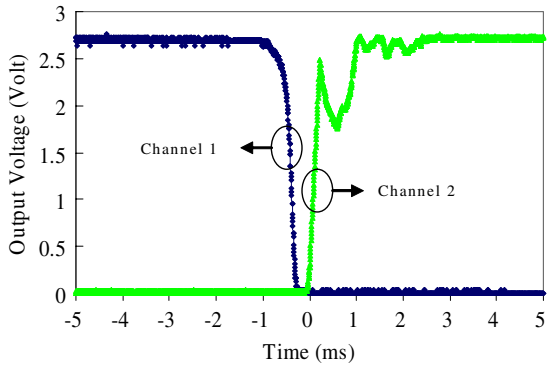

Figure 12. Measured switching behaviors. The transient curves are the measured photo-diode output voltages of channels 1 and 2.

setup shown in figure 8(*b*). As shown in figure 12, the input fiber, which originally aligns with the output fiber of channel 1, switches to (align with) the output fiber of channel 2. The oscillation of the channel 2 signal arises from the bouncing effect when the fiber-holding table and the stopper collides each other. This bouncing effect disappears within 2.5 ms. The total switching time (including the bouncing effect) is about 3.5 ms. The measured values of insertion losses and switching time are lower than the BELLCORE requirements which are listed in table 3.

Table 3. The measured values of insertion losses and switching time versus the BELLCORE requirements.

	Measured values		
Parameters	Channel 1	Channel 2	BELLCORE
Insertion loss (dB)	0.92	0.89	<1
Switching time (ms)	3.5		<20

5. Conclusions

In this work, an optical fiber-switching design, which consists of comb-drive actuators and folded-beam suspended structures, is designed and fabricated. The proposed design includes a mechanism which can effectively reduce the axial and angular misalignment associated with butt coupling. We also propose a dual-thickness SOI process which can be used to fabricate the suspended microstructure with two different structure thicknesses. The measured average insertion losses for the two output channels of the switch are 0.92 dB and 0.89 dB, respectively. Also, the measured switching time is about 3.5 ms.

Acknowledgments

This work was partially supported by the National Science Council, Taiwan, Republic of China (contract no. NSC 93-2212-E-002-023). The authors would like to thank Mr Sun-Chih Shih and Mr Shen-An Yang for their help with device packaging.

References

[1] Bourouha M A, Bataineh M and Guizani M 2002 Advances in optical switching and networking: past, present and future *Proc. IEEE Southeast Conf. (Columbia, SC, USA)* pp 405–13

[2] Dautartas M F, Benzoni A M, Chen Y C, Blonder G E, Johnson B H, Paola C R, Rice E and Wong Y-H 1992 A silicon-based moving-mirror optical switch *J. Lightwave Technol.* **10** 1078–84

[3] Field L A, Burriesci D L, Robrish P R and Ruby R C 1995 Micromachined 1 × 2 optical fiber switch *Transducers'95: Proc. 8th Int. Conf. Solid-State Sensors and Actuators (Stockholm, Sweden)* pp 344–7

[4] *Datasheet of Single Mode Single Fiber Collimator* 2004 Koncent Inc.

[5] *Product Information of Corning OptiFocus™ Collimating Lensed Fiber* 2003 Corning Inc.

[6] Yang Y, Liu W, Wu Y, Yang J and Wang Y 2004 Novel MEMS torsional mirror optical switch *Proc. SPIE* **5281** 718–26

[7] Li J, Zhang Q X and Liu A Q 2003 Advanced fiber switches using deep RIE (DRIE) fabrication *Sensors Actuators* A **102** 286–95

[8] Hoffmann M, Kopka P and Voges E 1999 Bistable micromechanical fiber-optic switches on silicon with thermal actuators *Sensors Actuators* A **78** 28–35

[9] Kanamori Y, Aoki Y, Sasaki M, Hosoya H, Wada A and Hane K 2005 Fiber-optical switch using cam-micromotor driven by scratch drive actuators *J. Micromech. Microeng.* **15** 118–23

[10] Bhuiyan Md M I, Haga Y and Esashi M 2005 Design and characteristics of large displacement optical fiber switch *IEEE J. Quantum Electron.* **41** 242–9
[11] Nagaoka S and Suzuki Y 1997 Compact optomechanical switches and their applications in optical communication and testing systems *MEMS'97: IEEE Proc. Micro Electro Mechanical System (Nagoya, Japan)* pp 366–71
[12] Hoffmann M, Nuesse D and Voges E 2003 An electrostatically actuated 1 × 2 moving-fiber switch *IEEE Potonics Technol. Lett.* **15** 39–41
[13] Pieri F and Piotto M 2000 A micromachined bistable 1 × 2 switch for optical fibers *Microelectron. Eng.* **53** 561–4
[14] Gonzalez C and Collins S D 1997 Magnetically actuated fiber-optic switch with micromachined positioning stages *Opt. Lett.* **22** 709–11
[15] Norwood R A, Holman J and Shacklette L W 1998 Fast, low insertion-loss optical switch using lithographically defined electromagnetic microactuators and polymeric passive alignment structures *Appl. Phys. Lett.* **73** 3187–9
[16] Minotti P, Le Moal P, Joseph E and Bourbon G 2001 Toward standard method for microelectromechanical systems material measurement through on-chip electrostatic probing of micrometer size polysilicon tensile specimens *Japan. J. Appl. Phys.* **40** L120–2
[17] Tang W C, Nguyen T-C H and Howe R T 1989 Laterally driven polysilicon resonant microstructures *Sensors Actuators* A **20** 25–32
[18] Legtenberg R, Groeneveld A W and Elwenspoek M 1996 Comb-drive actuators for large displacements *J. Micromech. Microeng.* **6** 320–9
[19] Gere J M and Timoshenko S P 1990 *Mechanics of Materials* 3rd edn (Boston, MA: PWS-Kent)
[20] Juan W-H and Pang S W 1998 High-aspect-ratio Si vertical micromirror arrays for optical switching *J. Microelectromech. Syst.* **7** 207–13
[21] Technical Reference TR-NWT-001221 *Generic Requirements for Fiber Optic Switches* Issue 1, Jan. 1994, BELLCORE
[22] Laermer F and Schlip A 1996 Method of anisotropically etching silicon *USA Patent No* 5501893